Journal of Rock Mechanics and Geotechnical Engineering 5 (2013) 110–123

Journal of Rock Mechanics and GeotechnicalEngineering

Journal of Rock Mechanics and Geotechnical Engineering

journal homepage: www.rockgeotech.org

Impact of stress on solute transport in a fracture network: A comparison study

Zhihong Zhao[a,*], Jonny Rutqvist[b], Colin Leung[c], Milan Hokr[d], Quansheng Liu[e,f], Ivars Neretnieks[a], Andrew Hoch[g], Jiří Havlíček[d], Yuan Wang[b,h], Zhen Wang[b,i], Yuexiu Wu[f], Robert Zimmerman[c]

[a] *Royal Institute of Technology, Stockholm, Sweden*
[b] *Lawrence Berkeley National Laboratory, Berkeley, USA*
[c] *Imperial College, London, UK*
[d] *Technical University of Liberec, Czech Republic*
[e] *Institute of Rock and Soil Mechanics, Chinese Academy of Sciences, Wuhan, China*
[f] *Wuhan University, Wuhan, China*
[g] *Serco TAS, Didcot, UK*
[h] *Hohai University, Nanjing, China*
[i] *Tongji University, Shanghai, China*

ARTICLE INFO

Article history:
Received 1 April 2012
Received in revised form 21 October 2012
Accepted 19 November 2012

Keywords:
Fractured rocks
Solute transport
Discrete element method
Equivalent continuum
Dual-porosity model
Particle tracking method

ABSTRACT

This paper compares numerical modeling of the effect of stress on solute transport (advection and matrix diffusion) in fractured rocks in which fracture apertures are correlated with fracture lengths. It is mainly motivated by the performance and safety assessments of underground radioactive waste repositories. Five research teams used different approaches to model stress/deformation, flow and transport processes, based on either discrete fracture network or equivalent continuum models. The simulation results derived by various teams generally demonstrated that rock stresses could significantly influence solute transport processes through stress-induced changes in fracture apertures and associated changes in permeability. Reasonably good agreement was achieved regarding advection and matrix diffusion given the same fracture network, while some observed discrepancies could be explained by different mechanical or transport modeling approaches.

1. Introduction

The performance/safety assessment of deep underground repositories of radioactive nuclear waste requires the knowledge and understanding of coupled mechanical and transport processes in fractured rocks, including the stress effects on radio nuclides migration in porous and fractured rocks. This topic is also important in other energy engineering and environmental protection projects, such as groundwater pollution and oil/gas production from fractured reservoirs. However, experimental investigation of the stress impact on solute transport in fractured rocks involving a complex and realistic fracture network is almost impossible at present, mainly due to the technical difficulties in realizing fracture systems and carrying out the experiments under well-controlled laboratory and in situ test conditions.

In the past three decades, stress effects on fluid flow through single fractures or fractured rocks have been investigated by numerical modeling (e.g. Oda, 1986; Bai and Elsworth, 1994; Zhang and Sanderson, 1996; Chen and Bai, 1998; Bai et al., 1999; Koyama et al., 2006). Important progress was made more recently by Jing and his co-workers (Min et al., 2004a,b; Baghbanan and Jing, 2008). Their results indicate that fracture conductivity or equivalent permeability of fractured rocks, as well as flow patterns (channeling), can be significantly changed under various stress conditions. Due to the fact that solute transport strongly depends on the fluid flow conditions in the fractured rocks, it is expected that the stresses could also play an important role in solute migration. However, to the authors' knowledge there are only a few publications concerning the stress (or engineering perturbations) effects on solute or particle transport processes in single rock fractures (Moreno et al., 1988; Jeong and Song, 2005; Koyama et al., 2008) or fractured rocks (Zhao et al., 2011; Genty et al., 2011; Waber et al., 2011), and modeling the coupled stress-flow-transport processes in fracture networks has rarely been attempted.

* Corresponding author. Tel.: +46 8 7908661.
E-mail address: zhzhao@kth.se (Z. Zhao).

Peer review under responsibility of Institute of Rock and Soil Mechanics, Chinese Academy of Sciences.

Production and hosting by Elsevier

1674-7755
http://dx.doi.org/10.1016/j.jrmge.2013.01.002

The main objective of this study is to investigate the state-of-the-art of numerical modeling approaches and techniques for characterizing and understanding the influences of stress/deformation on solute migration in fractured crystalline rocks, where fluid flow is dominated by connected fracture networks, considering a realistic representation of fracture network geometry and stress-deformation behaviors of the fractures (Hudson et al., 2009). This study was conducted as a part of the international DECOVALEX-2011 project, Task C, and there were five research teams working on this problem: Imperial College London (IC) and Lawrence Berkeley National Laboratory (LBNL), in collaboration with Serco TAS and supported by the Nuclear Decommissioning Authority (NDA), UK; Royal Institute of Technology (KTH), supported by Swedish Nuclear Fuel and Waste Co. (SKB), Sweden; Technical University of Liberec (TUL), supported by Radioactive Waste Repository Authority (RAWRA), Czech Republic; and Institute of Rock and Soil Mechanics, Chinese Academy of Sciences (CAS), China. This paper briefly describes the numerical models (in Section 3) used by five teams for simulation of the coupled stress-flow-transport processes and then compares the corresponding results in Section 4.

2. Benchmark test definition

The modeling study is centered around a benchmark test (BMT), which was defined based on a problem of fracture network studied by Baghbanan and Jing (2007, 2008). The original objective in Baghbanan and Jing (2007, 2008) was to evaluate the equivalent hydraulic permeability of the two-dimensional (2D) fracture system, with model dimensions from 0.25 m to 20 m, so that many small fractures were included in the models. For the current modeling study, the model domain is 20 m by 20 m, and contains 7797 fractures of various lengths and apertures (Fig. 1). Each individual research team could decide whether those very small fractures would be included, according to their own judgment, necessary simplification measures, and fracture characterization concepts. Different approaches, either discrete fracture or equivalent continuum models, could be chosen, including necessary homogenization schemes for handling the fractures.

For the BMT problem, the material properties of the fractures and intact rocks were defined according to Table 1. The rock matrix was assumed to be linear, isotropic, homogeneous and elastic, characterized by Young's modulus and Poisson's ratio. Fluid flow in the rock fractures was assumed to follow the cubic law. The normal deformation of the fractures was assumed to follow a Barton–Bandis model, with a hyperbolic non-linear stiffness k_n (Baghbanan and Jing, 2008):

$$k_n = \frac{(\sigma_{nc} + 10\sigma_n)^2}{9\sigma_{nc}a_0} \tag{1}$$

where $\sigma_{nc}\,(\mathrm{MPa}) = 0.487a_0\,(\mu\mathrm{m}) + 2.51$ is the critical normal stress; σ_n is the normal compressive stress; and a_0 is the initial aperture of the fracture at zero normal stress. The values of a_0 correlated with fracture trace lengths, following an equation given by Baghbanan and Jing (2007), were provided to the teams. According to the Barton–Bandis hyperbolic normal closure model, the normal stress versus normal displacement relationship can be defined as

$$u_n = \frac{9\sigma_n a_0}{\sigma_{nc} + 10\sigma_n} \tag{2}$$

where u_n is the fracture normal displacement.

In the shear direction, an elastic-perfectly plastic model with a Mohr–Coulomb failure criterion was defined, assuming a constant shear stiffness, for simplicity. After shear failure is reached, the continued shear displacement, u_s, was related to the shear dilation, u_d, by a constant dilation angle, φ_d, according to

$$u_d = u_s \tan\varphi_d \tag{3}$$

The shear dilation is then added to the normal stress-dependent fracture aperture (Eq. (2)), assuming that the mechanical and hydraulic apertures are equal, for simplicity.

The stress effects on solute transport in fractured rocks were investigated according to the following procedure. Firstly, various boundary stresses (Fig. 2) were applied to the model (Fig. 1) to

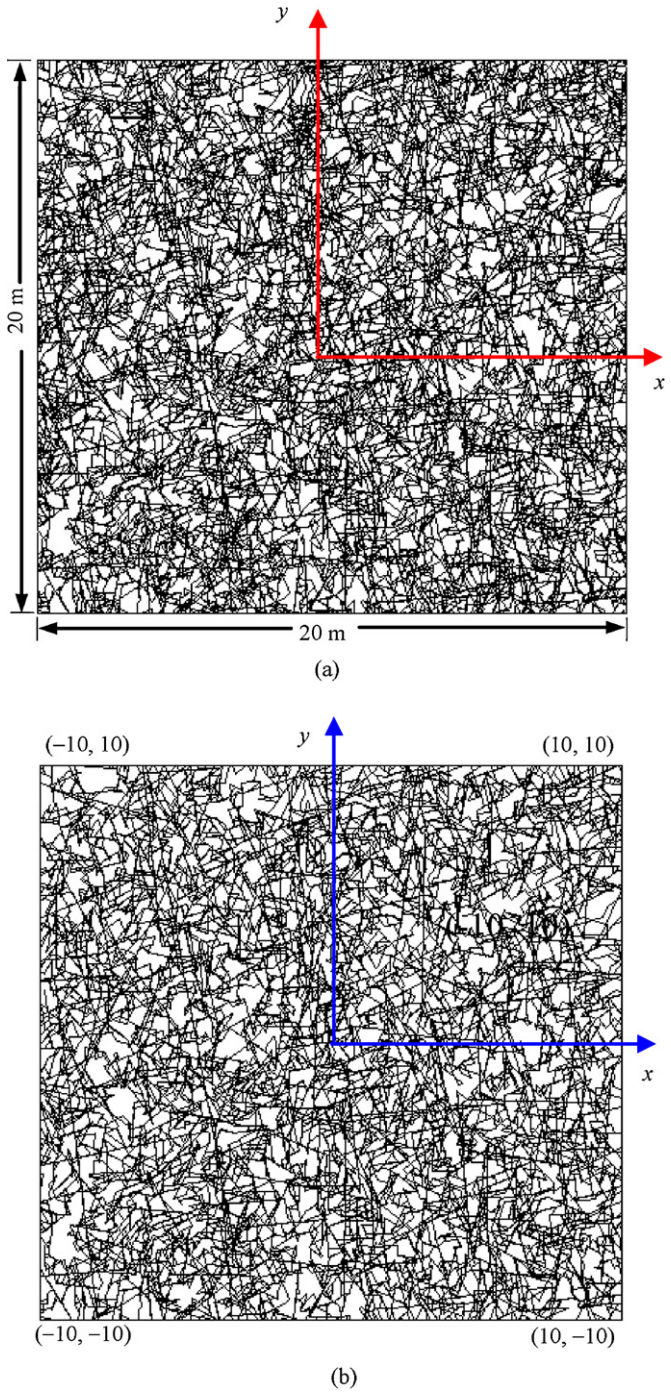

Fig. 1. Model geometry after regulation. IC and TUL used the original fracture network. KTH simplified the original fracture network by removing some small fractures. LBNL used the original fracture network for calculation of equivalent, dual-continuum properties. (a) Original model. (b) Simplified model by KTH.

Table 1
Physico-mechanical properties of intact rock and fractures.

Intact rock						Fractures			
Elastic modulus (GPa)	Poisson's ratio	Shear stiffness, K_s (GPa/m)	Friction angle (°)	Dilation angle (°)	Cohesion (MPa)	Critical shear displacement for dilation, u_{cs} (mm)	Mean fracture aperture (μm)	Residual aperture (μm)	Maximum aperture (μm)
84.6	0.24	434	24.9	5	0	3	65	1	200

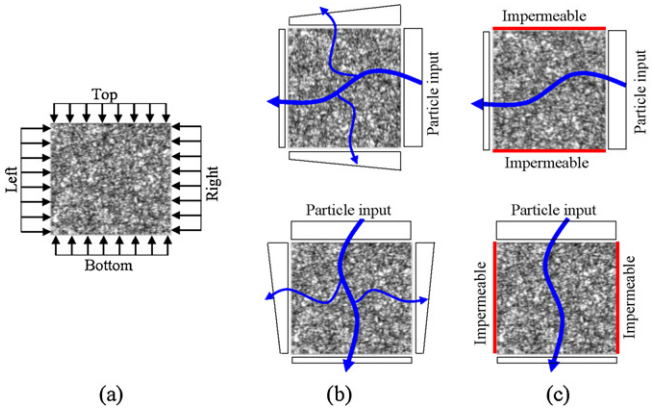

Fig. 2. Boundary conditions. (a) Stress conditions. (b) Three outlet boundaries. (c) One outlet boundary.

generate the deformed models for later fluid flow and transport analysis. A constant vertical normal compressive stress of 5 MPa was specified at the top and bottom boundaries, and the horizontal normal compressive stresses, varying from 5 MPa, 10 MPa, 15 MPa to 25 MPa, were applied at the left and right boundaries. In this way, the stress ratio, defined as K = horizontal/vertical stresses, increased from K = 0, 1, 2, 3 to 5 stepwise (K = 0 represents the free state in which both horizontal and vertical stresses are zero).

Fluid flow through the model under various stress ratios was simulated by the specified hydraulic pressure, as illustrated in Fig. 2b and c. The hydraulic conditions allowed the fluid and solute to exit from the lateral sides that are aligned in the macroscopic flow direction, referring to as "three outlet boundaries", and the cases with closed (impermeable) lateral sides, called "one outlet boundary", were also studied. Two sets of hydraulic conditions were defined to obtain the macroscopic flow in the vertical and horizontal directions, respectively. The hydraulic pressure gradient was fixed at 10^4 Pa/m, and the hydraulic pressure at the center of the model was 2.0×10^5 Pa. Because the hydraulic gradient of 10^4 Pa/m is much higher compared with the expected conditions at a site of an underground radioactive waste repository, additional scenarios for both advection and matrix diffusion were carried out under a lower hydraulic gradient of 10 Pa/m that is closer to the expected hydraulic conditions.

The solute transport through the model was initially defined in terms of particle tracking. Three of the five teams did employ the particle tracking approach, while two other teams used a regular solute transport simulation approach. In particle tracking, solute particles were introduced at each inlet location in proportion to the flow rate at that point. This was equivalent to injecting a traced solution with constant concentration. The numbers of injected particles at the inlet boundary were determined by various teams according to their tools and models. The particles moving with the flowing fluid through the fracture network followed the flow paths (connected fractures) randomly, which implies that particles starting from the same point might end up in different exit points. Initially, only pure advection by fluid flow in fractures was considered. The concentrations of particles collected at the outlet boundary as function of time were reported in the form of breakthrough curves.

Output results were defined to be evaluated and compared in terms of total flow-through and equivalent permeability, and breakthrough curves, as well as other parameters that reflect the solute transport characteristics through numerical experiments under various stress conditions.

3. Methodologies

Either discrete fracture network (DFN) or equivalent continuum (EC) models were applied to simulate flow and transport processes in fractured rocks by different teams through various codes (Table 2). Moreover, as mentioned, both particle tracking and regular solute transport analyses were used by the different teams. In the following section, the techniques for fracture system characterization, and the algorithms used to simulate the stress effect, flow calculation and solute transport employed by various teams are described in detail.

3.1. IC team

The IC team carried out the simulations using NAPSAC, based on a direct representation of the discrete fractures making up the flow-conducting network (Serco, 2008). The far-field stress is projected individually onto each fracture, but the effects of stress concentration and interaction between fractures are not considered. The exact normal stress/displacement relationship defined in Eq. (2) was used. The shear behavior of fractures was described separately in two regions: below and above the critical shear stress, respectively (Fig. 3). If the shear stress applied on the fractures was below the critical shear stress (Region 1 in Fig. 3), no shear dilation occurred due to the shear displacement. The stiffness of each fracture changes before and after critical shear stress, K_{s1} and K_{s2}, respectively. Stiffness before slip comprises two parts: K_s^{fracture}, which is the stiffness given in the task definition (434 GPa), and K_s^{rock}, which is the elastic shear resistance of the surrounding rocks. From the literature on induced seismicity and earthquakes, K_s^{rock} can be expressed in a general form as $K_s^{\text{rock}} = \eta G/l$ (Dieterich and Linker, 1992; Rahman et al., 2002), where G is the shear modulus of the surrounding rock mass (34.1 GPa, estimated from the task definition), l is the half-length of the fracture, and η is a geometric constant relating to the geometry of the fracture (here assumed to be 0.92). Before slip, we have $K_{s1} = K_s^{\text{fracture}} + K_s^{\text{rock}}$, while after slip $K_{s2} = K_s^{\text{rock}}$. When the shear stress was above the critical shear stress (Region 2 in Fig. 3), slip occurred and the fracture's own shear stiffness became zero, so that the shear stiffness of the system only depended on the shear modulus of the surrounding rocks.

To simulate the steady-state constant-density groundwater flow in a fracture network, NAPSAC assumed the fracture transmissivity was related to the fracture aperture by the cubic law (Zimmerman and Bodvarsson, 1996), and the fluid flow rate in each fracture segment was determined numerically by a Galerkin finite

Table 2
Numerical codes applied by the teams.

Team	Code	Conceptual model and methods	Stress distribution algorithm
IC	NAPSAC	DFN particle tracking method (PT)	Stress projection
KTH	UDEC+PTFR	Discrete element method (DEM) PT	Direct solution of stress-flow coupling in DEM
TUL	FLOW123D	Combined of DFN and dual-porosity model FVM and solute transport	Stress projection
LBNL	TOUGH+FLAC	Equivalent continuum, crack tensor theory and solute transport	Stress projection
CAS	UDEC+TDRW_PACKAGE	Discrete element method (DEM) TDRW particle tracking method	Direct solution of stress-flow coupling in DEM

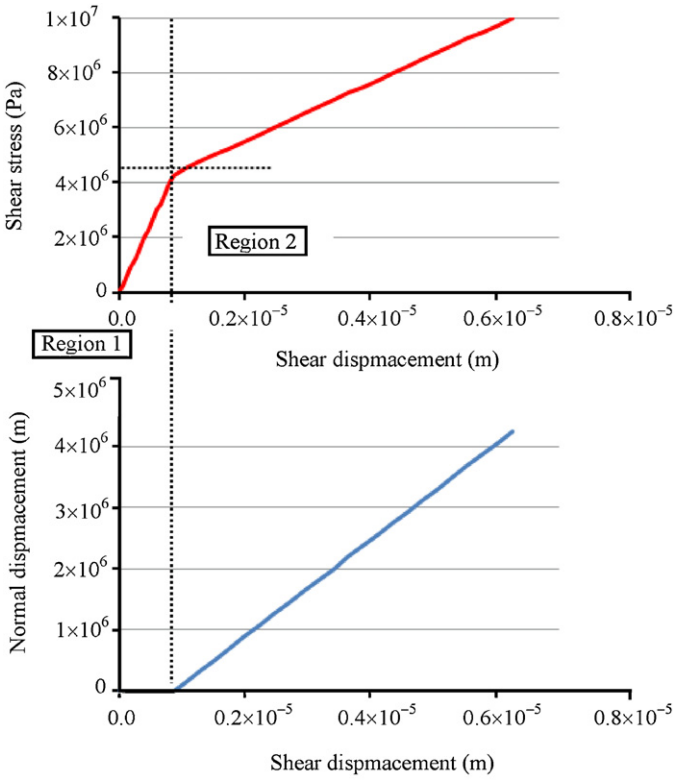

Fig. 3. Strategy for modeling shear dilation used by IC team.

element approach. Full details of this algorithm were given in the NAPSAC technical summary (Serco, 2008).

NAPSAC simulated the solute transport through a fracture network by particle tracking method. It was assumed that advection was dominating within the single fractures (i.e. negligible molecular diffusion), and the fracture apertures were small enough that the tracer diffused quickly across the apertures (i.e. equal concentration in each fracture section). Note that the above assumptions were also applicable for the KTH model. For each fracture, a representative number of path lines between its intersections with other fractures were calculated. The intersections were split up by transport nodes, and the path lines were calculated from each transport node. A "mass conserving method", which used the algorithm of Cordes and Kinzelbach (1992) to conserve mass among finite elements, was implemented in NAPSAC and used in this study. For a large swarm of particles through the network, the particles could be injected on any inflow surfaces of the model region, or on an engineered feature. The particles were then tracked through the network from transport node to transport node, building up the path taken by each particle using the path line information calculated previously.

In fractured rocks with a porous rock matrix (e.g. granite), the particles might also diffuse into and out of the rock matrix, when they migrated along with the groundwater in the fractures. This process is known as rock matrix diffusion (RMD), and could retard the particles (i.e. increase their travel times) considerably. A Laplace transform method was used in NAPSAC to calculate the extra "retarded" travel times due to RMD for the path lines in each fracture. Some further details and verification of the method were given by Hoch (1998). An important parameter called the "diffusion distance", representing the average fracture spacing, must be specified in the NAPSAC model.

3.2. KTH team

In the KTH models, the rock matrix was represented by an assembly of discrete deformable, but impermeable blocks, with fractures represented as the interfaces between the distinct blocks, were idealized by the parallel plate model. To obtain the flow field under different stress and hydraulic conditions, a 2D discrete element code, UDEC, was used. Details of the numerical stress-flow calculation procedures can be found in other publications (Itasca, 2004; Min et al., 2004b; Baghbanan and Jing, 2008). The normal deformation of the fractures followed a simplified stepwise function (Fig. 4a) to approximate the non-linear normal stress-normal closure relationship described by Eq. (2). In shear, the response was described by an elastic-perfectly plastic constitutive model with a Mohr–Coulomb failure criterion (cohesion (c) and frictional angle (φ)). The shear dilation occurred at the onset of slip (non-elastic sliding) of fractures (Eq. (3) and Fig. 4b). The accumulated dilation was generally limited by either a high normal stress level or by a large accumulated shear displacement that exceeded a limiting value, u_{cs}.

The mass continuity equation was solved at fracture intersections through an iterative scheme under the prescribed hydraulic boundary conditions to obtain the flow field. In the UDEC code, the fluid pressure in the "domains" was calculated, where "domains" are the region of space between blocks (i.e. fracture intersections) defined by the contact points. The fluid flow was then governed by the pressure gradient between adjacent domains. The flow rate per unit width of fractures followed the cubic law as described in IC model. The current hydraulic aperture considering stress effects was given by

$$a = a_0 - u_n + u_d \tag{4}$$

A residual value $a_{res} = 1\,\mu m$ and the maximum value $a_{max} = 200\,\mu m$ were assumed for apertures to improve the efficiency of calculations, below and beyond which mechanical closure does not affect the fracture permeability (Itasca, 2004).

Basically, the KTH team followed the methodologies suggested in the technical definition to simulate the solute transport by particle tracking method (Neretnieks et al., 2009). In each fracture segment, the water residence time, t_w^i, was calculated by

$$t_w^i = \frac{V_i}{Q_i} \tag{5}$$

where V_i is the volume of fracture leg i, i.e. the product of the length L_i, the width W_i and the aperture b_i; and Q_i is the flow rate calculated by the cubic law. For 2D cases, W_i is assumed to be a unit value of 1 m. According to the assumption of complete mixing at fracture

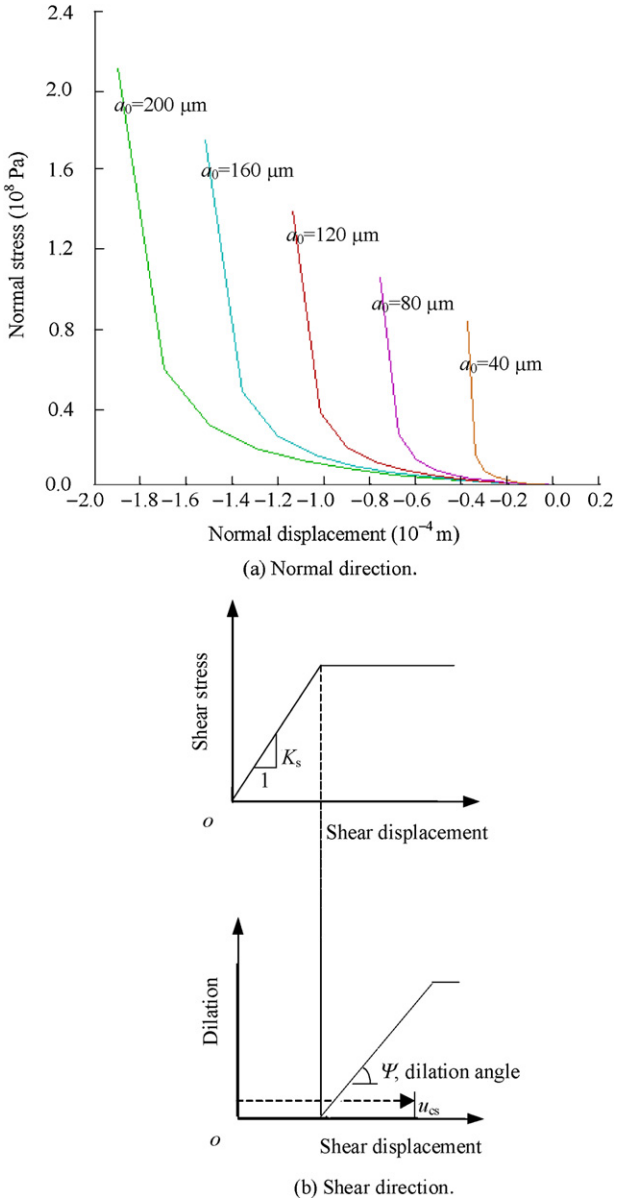

Fig. 4. Constitutive models of fracture mechanical behavior used by KTH team. (a) The horizontal axis represents normal displacement (negative for closure). For different initial apertures, the nonlinear normal stiffness varies, but increases with normal displacement. (b) Shear dilation, occurring at the onset of slip of fracture, is described by a constant dilation angle Ψ.

intersections, the particles were fully mixed with fluids and with each other, so that their probability of going forward to any one of the outlet fractures connected to that intersection was proportional to its flow rate. This was the way how the particles left the fracture intersection and entered the next fracture leg. Consequently, the total water residence time, t_w^k, for a particle k, was the sum of the water residence time of this particle in all the fracture segments it passed:

$$t_w^k = \sum_i t_w^i = \sum_i \frac{V_i}{Q_i} \tag{6}$$

To consider the effects of matrix diffusion and sorption on inner matrix surfaces, the total residence time for each particle k, t^k, could be obtained for a step input with an initial concentration, c_0, at time zero (Moreno et al., 2006; Neretnieks et al., 2009):

$$\frac{c}{c_0} = erfc\left[\frac{1}{2}\left(\frac{A_q}{Q}\right)^k \frac{MPG}{(t^k - t_w^k)^{0.5}}\right] \tag{7}$$

where $(A_q/Q)^k$ is the ratio of flow wetted surface (FWS) to flow rate, which is further determined by $(A_q/Q)^k = \sum_i 2L_i W_i/Q_i$; and MPG (materials property group) is assumed constant containing information on pore diffusivity D_p, sorption coefficient K_m and matrix porosity ε_p. A large value of $(A_q/Q)^k$ allowed the particles to access the pore water in the rock matrix by diffusion and thus gave the particles more water to reside in than if it only had access to the flowing water in the fracture.

When matrix diffusion was included, there was a residence time distribution given by Eq. (7), instead of the single water residence time for a particle (Eq. (6)). To incorporate the effects of matrix diffusion into particle tracking method, a random number, R, from the uniform interval [0,1] was chosen to equal the c/c_0 in Eq. (7) (Yamashita and Kimura, 1990):

$$[R]_0^1 = erfc\left[\frac{1}{2}\left(\frac{A_q}{Q}\right)^k \frac{MPG}{(t^k - t_w^k)^{0.5}}\right] \tag{8}$$

and thus the total residence time for this particle can be obtained by

$$t^k = t_w^k + \frac{1}{4}\left[\left(\frac{A_q}{Q}\right)^k \frac{MPG}{erfc^{-1}([R]_0^1)}\right]^2 \tag{9}$$

Based on an earlier computer code "CHAN3D" (Gylling et al., 1999) for tracking particle movement through regular channel networks, we developed a code, PTFR, for particle migration in irregular 2D fracture network based on the fluid flow results obtained by UDEC, in association with the same concepts of "contact" and "domain" used in the UDEC data structure. More details can be also found in Zhao et al. (2011).

3.3. TUL team

The TUL team used FLOW123D (TUL, 2011) to simulate flow and transport in fractured rocks. Since FLOW123D had no mechanical capabilities, the stress and deformation were calculated analytically and independently for each fracture. The normal and tangential stresses applied on the fractures were estimated by simple stress (force) projection:

$$\sigma_n = \sigma_x \sin^2\alpha + \sigma_y \cos^2\alpha \tag{10}$$

$$\tau = \sigma_x \sin\alpha\cos\alpha - \sigma_y \sin\alpha\cos\alpha \tag{11}$$

where σ_x and σ_y are the boundary stresses in the x- and y-directions, respectively; and α is the angle between the fracture and x-axis (evaluated in the interval $[-90^\circ, 90^\circ]$, corresponding to unsigned normal vector, i.e. the 180° rotated fracture is regarded as identical). In the normal direction, Eq. (2) was used to describe the aperture changes due to the normal stresses. For shear displacement, only the part after slip, u_s^s, was assumed to contribute to the dilation, and the corresponding shear dilation is

$$u_d = \min(u_s^s, u_{cs})\tan\varphi_d \tag{12}$$

Note that the above u_{cs} did not include the elastic shear displacement, which was different from the KTH model, but the difference of inclusion or exclusion of the elastic shear displacement in u_{cs} was negligible. Finally, the aperture could be evaluated additively with appropriate sign (Eq. (4)).

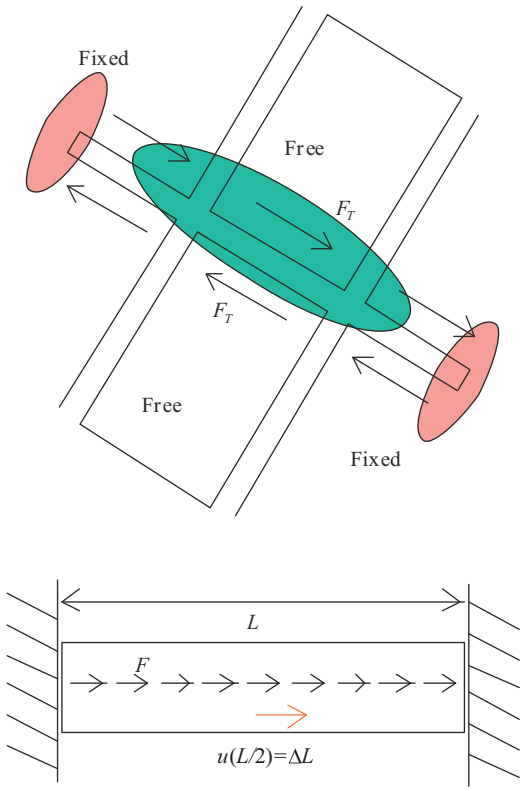

Fig. 5. Mechanical model of individual fracture for tangential stress–displacement relation in TUL models.

To represent the relationship of shear stress/shear displacement after slip, a weak elastic relation (smaller stiffness) in the slip regime was proposed in the TUL model, which is similar to the IC model (Region 2 in Fig. 3). Taking into account the possible constraints from the intact rocks formed by the fractures (Fig. 5), the following assumptions were applied in the TUL model: (1) the sliding blocks were fixed at the end of the fracture, due to the fact that the rock matrix is order-of-magnitude more stiff; (2) the normal deformation in the perpendicular fractures was negligible (10 μm versus 100 μm orders of magnitude); (3) even if the derived displacement was a maximum value in the center of fracture, this value was considered as a constant for whole fracture length L in the consequent aperture change calculation. Therefore, the fracture as two sliding blocks fixed at the ends was mechanically analogous to the uniaxial model of a bar of length L and cross-section area S with supports on both ends loaded with distributed axial force (Fig. 5), and the equivalent shear displacement ΔL and stiffness τ_s were

$$\Delta L = \frac{FL}{8ES} = \frac{\tau_s L}{8E} \tag{13}$$

$$k_{s,2} = \frac{\tau_s}{\Delta L} = \frac{8E}{L} \tag{14}$$

The length-dependent shear stiffness could be set with different Young's moduli E of intact rock (weaker for the intact rock due to other crossing fractures). $E = 2000$ GPa was chosen to obtain significant fracture opening in the large stress anisotropy case as in Min et al. (2004b), denoted as "TUL_1" hereafter. The other case denoted as "TUL_2" set the shear stiffness relation $k_s = 31.2\,\text{GPa}/(2L)$, which is the same value as used in the IC model.

The TUL model of flow is in principle a discrete fracture network with the standard cubic law applied in each fracture segment, and with the assumption of pressure continuity in fracture crossings.

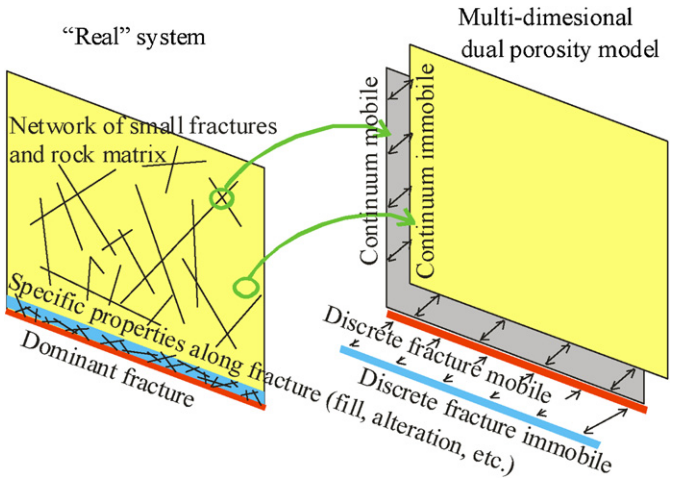

Fig. 6. Scheme of interpretation of each dimension of multi-dimensional model with immobile zones in FLOW123D.

They used an in-house-developed code FLOW123D, which is based on a more general conceptual model: combining the ideas of an equivalent continuum model, discrete fracture network and double-porosity model to simulate flow and transport processes in fractured rocks, with a system of 3D continuum, 2D discrete fracture network and a network of 1D fracture intersections. Each part was further composed of mobile and immobile parts (double continuum in Fig. 6): (1) 3D mobile zone: rock pores, equivalent continuum representation of small fractures; (2) 3D immobile zone: dead-end pores in rock, immobile zone of double porosity representation of small fractures; (3) 2D mobile zone: discrete fracture network of large fractures, or representation of planar structures of similar behavior (e.g. a fracture zone as a single plane in a larger scale), in case of such representation is by double porosity model, only the mobile zone is regarded; (4) 2D immobile zone: dead-end pores if the fracture is filled with minerals, immobile zone of the representation of a general planar structure with the single-plane double-porosity model (above); (5) 1D mobile zone: intersections of discrete fractures; (6) 1D immobile zone: like 2D immobile zone in the 2D model geometry with 1D fractures (not a typical case in 3D models).

The fluid flow in each subdomain (dimension) was governed by the Darcy-type law, i.e. potential flow in each 1D, 2D and 3D domain. This was consistent with the standard Darcy's law for a 3D continuum, and with the Hagen–Poiseuille law for flow in open fractures, with appropriate real or equivalent hydraulic conductivity. The interaction between domains was consistently represented by a corresponding linear flux-pressure relation, either it can represent fracture surface coating or it is needed to connect the discrete elements in different places (effect of numerical discretization even for continuous pressure between fracture and rock matrix), but is not used for connection of 1D elements in the same point in this work. The transport problem was governed by the advection–dispersion equation coupled with a linear law of non-equilibrium exchange between mobile and immobile zones. The transport between the 1D, 2D and 3D domains was included in the advection term. Nuclear and chemical reactions were represented as additional source terms in both zones. More details about the method can be found in Maryška et al. (2008). In the presented study, only advection is considered.

To compare with the particle tracking method in DFN models (IC and KTH models), the total outflow mass in one time step corresponded to the mass of exiting particles in particle tracking method, so this mass could be assigned an attribute of the current simulation

time, i.e. the actual residence time of that total mass. Therefore, the mean residence time, *MRT*, and the residence time variance, *VAR*, could be determined, respectively, as

$$MRT = \frac{\sum_{i=1}^{N}(\sum_j c_j Q_j)_i \Delta t t_i}{\sum_{i=1}^{N}(\sum_j c_j Q_j)_i \Delta t} \tag{15}$$

$$VAR = \frac{\sum_{i=1}^{N}(\sum_j c_j Q_j)_i \Delta t (t_i - MRT)^2}{\sum_{i=1}^{N}(\sum_j c_j Q_j)_i \Delta t} \tag{16}$$

where i is the individual time step, j is the individual elements (single fractures), c_j is the concentration in the jth element (fracture), Q_j is the flow rate through the element wall (fracture boundary point in 2D), Δt is the length of time step, t_i is the simulation time in the ith step (i.e. $t_i = i\Delta t$), and N is the number of time steps.

Calculation of A_q/Q in continuous form (integral instead of sum) was described by the equation of reactive transport with a value of zero order reactions $2/a$:

$$\frac{\partial X}{\partial t} + \nabla \cdot (Xv) - \nabla \cdot (D \nabla X) = \frac{2}{a} \tag{17}$$

where A_q/Q is specified as quantity X, and a is the fracture aperture. Then the mean value and variance of A_q/Q across individual trajectories and aggregates of mass over each time step could be determined, in the similar way for the residence time. This method also clearly showed the quantitative importance of A_q/Q. In narrow fractures with slow flow, the value of A_q/Q increased the most, while in wide fractures with a fast flow it decreased to the minimum. Compared with the particle tracking method used by IC and KTH, the TUL method could not obtain the details of each particle passing different paths through the area; it provided the data from the output fracture elements on the downstream boundary. So, they represented a set of paths starting from different positions on the input and ending in one common output. This led to a less detailed layout of flow wetted surface values, and made the histogram coarser.

3.4. LBNL team

The LBNL team applied a multi-continuum modeling approach with equivalent continuum properties calculated from the background fracture network, and a standard solute transport approach (not particle tracking). In Rutqvist et al. (2002), the approach, model developments, and applications for equivalent continuum and dual-continuum medium were described in detail. Basically, the 20 m × 20 m model domain was divided into square-shaped elements, including overlapping fracture and matrix continuum elements. The approach was applied using the TOUGH-FLAC simulator (Rutqvist et al., 2002; Rutqvist, 2011), which is based on linking the TOUGH2 multiphase flow simulator (Pruess et al., 1999) with the FLAC^{3D} geomechanical simulator (Itasca, 2009). The multiple-interaction continuum (MINC) approach available in the TOUGH2 multiphase flow simulator was employed (Fig. 7). The equivalent properties (such as the permeability and elasticity tensors) were calculated for each fracture continuum element (Fig. 8). Two different methods were applied and tested for calculating the equivalent hydraulic properties (permeability tensor and porosity): (1) using numerical DFN flow calculations according to Jackson et al. (2000), and (2) analytically evaluated using Oda's crack tensor theory (Oda, 1986). In Rutqvist et al. (2002), they investigated the effect of the element size for cases dividing the 20 m × 20 m model into 400 × 400, 100 × 100, 40 × 40, 10 × 10, and 4 × 4 elements. Thus, the size or side length of these elements are 0.05 m, 0.2 m, 0.5 m, 2 m, and 5 m, respectively. One can imagine that in the case of side length 0.05 m, only 1 or 2 fractures, or indeed none will intersect an element. In such case, the approach fractures are represented discretely through modification of properties of the elements that intersect a trace of a fracture. Such an approach was previously introduced and applied using TOUGH-FLAC in Rutqvist et al. (2009) for studies related to the excavation disturbed zone around tunnels in fractured rocks.

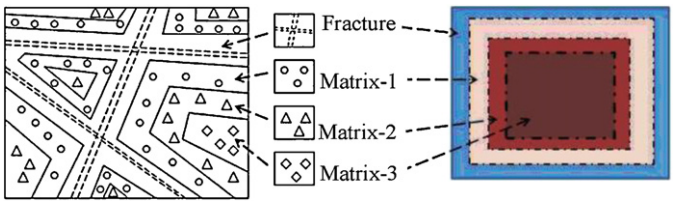

Fig. 7. Schematic diagrams for the multiple porosity model and MINC concept according to Pruess and Narasimhan (1985). Left: A composite porous medium which consists of several distinct types of porous materials. Right: A conceptual diagram for a MINC model (Kim et al., 2012).

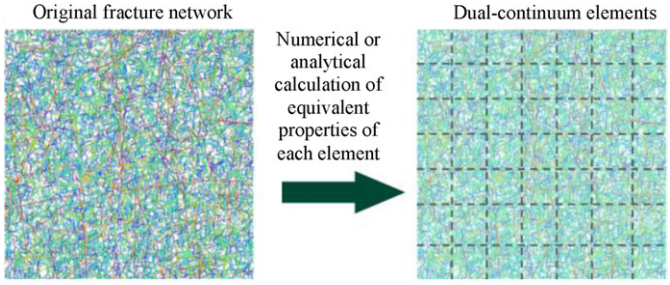

Fig. 8. Scheme of dual-continuum approach used by the LBNL. The original fracture network was simulated using overlapping fracture and matrix continua with equivalent properties of the fractured continuum elements calculated numerically using NAPSAC or analytically using Oda's crack tensor theory.

The LBNL team tested the approach of analytical evaluation of the permeability tensor (using Oda's crack tensor) and compared it with the numerically evaluated permeability tensor (Jackson et al., 2000), by comparing flow rates for both vertical and horizontal flow gradients. The LBNL team also compared with the flow results of NAPSAC DFN modeling described in detail in Section 3.2. The results of this comparison indicated some problems when using Oda's crack tensor theory "as is", specifically, when element sizes became small compared to the density of the fracture network. For example, in the case of 400 × 400 elements, the total flow through the 20 m × 20 m model became too small, amounting to about 70% of the DFN model results. The problem was identified to be due to the fact that (1) the element size was clearly smaller than REV, and (2) there was a reduction in flow related to the finite difference scheme in TOUGH2 (Rutqvist, 2011). When element size increased, the total flow rate through the model stabilized to value in reasonable agreement with the NAPSAC DFN simulation results. For the analytically evaluated equivalent properties and when using TOUGH2, the total flow rate through the 20 m × 20 m model stabilized to a good value for element side length of 0.5 m or larger (i.e. when the model was divided into 40 × 40 elements or fewer). On the other hand, when using numerically evaluated permeability tensor, as well as an alternative finite element flow simulator (NAMMU), the total flow through the 20 m × 20 m model was reasonably close to the NAPSAC DFN simulation results for all discretization tests (i.e. ranging from 4 × 4 to 400 × 400 elements). The problem with the analytically evaluated permeability and TOUGH2 finite difference scheme could be corrected considering special treatment of discrete fractures intersecting the element (Rutqvist, 2011). However, the LBNL simulation results presented in this paper are for the

40×40 elements case in which the analytically evaluated permeability tensor used "as is" and TOUGH2 produced a reasonable flow rate through the 20 m × 20 m fractured model domain. In terms of transport, equivalent continuum model with larger elements produces a more homogenous (smooth) permeability field that is expected to lead an underestimation of hydrodynamic dispersion compared with the original fracture network model.

The breakthrough curves were calculated using solute transport in which a different water (water 2) was supplied at one boundary in pulse for 10 s, and the water mass breakthrough at the three other boundaries was monitored. This approach to simulate transport is comparable with that of the TUL team. The stress effect on the permeability and elastic tensors was evaluated for each element considering stress-induced aperture changes for each fracture intersecting the element. This is similar to the approach used by the IC team, except that in the LBNL approach it was done individually for each element along a fracture trace. This method of calculating aperture changes for each fracture is equivalent to the approach taken by the IC team, using Eqs. (1) and (2). After calculating the new aperture for each fracture, the permeability tensor for each element is updated, reflecting the change in normal and shear stresses across each of the individual fractures that intersect the element.

Matrix diffusion was considered through the dual-continuum approach, in which water 2 will diffuse from fracture continuum elements to connected matrix continuum elements as a result of the concentration gradient between the fracture and matrix continuum elements. In the simulation results used for this model comparison, for the 40×40 element mesh, one matrix continuum element was used for each fracture continuum element. This implies a linear concentration gradient between the fracture continuum element and matrix continuum element, and the gradient depends on the adopted average fracture spacing for each element. An improved treatment of matrix diffusion can be achieved by assigning multiple matrix elements, as illustrated in Fig. 7. This would help to resolve steep concentration gradients that might exist near the fracture and matrix interfaces.

3.5. CAS team

The CAS team also used UDEC to simulate flow in fractured rock mass, which was the same code used by the KTH team. The rock matrix was deformable and impermeable, and the fracture was regarded as a parallel plate. UDEC code was used to do the hydro-mechanical calculations with different stress and hydraulic boundaries. The normal mechanical behavior of the fracture is shown in Fig. 9, and was listed in a table named "nstable" in UDEC. The shear mechanical behavior of the fractures was described by a Mohr–Coulomb-slip joint model. The dilation that occurs after the joint begins to slip was approximated as a linear function of the dilation angle with a dilation limit that is a function of the shear displacement. The flow simulation methodology in the UDEC code was the same as described by the KTH team (in Section 3.2).

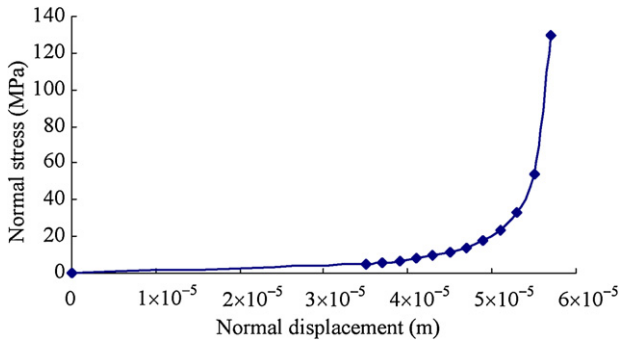

Fig. 9. Relationship between normal stress and normal displacement of fractures.

Solute transport was simulated using time domain random walk (TDRW) particle tracking method (Delay and Bodin, 2001; Bodin et al., 2003, 2007), in which fracture network was regarded as an assembly of connected fracture segments. The total water residence time, t_w^k, for a particle k, was the sum of the water residence time, Δt_f, of this particle in all the fracture segments it passed:

$$t_w^k = \sum_i t_w^i = \sum_i \Delta t_f \tag{18}$$

For matrix diffusion case, the residence time accounting for matrix diffusion, Δt_{fm}, was used in place of Δt_f in the above equation, where Δt_f and Δt_{fm} can be expressed, respectively, by

$$\Delta t_f = \exp(\mu_{\ln} + Z_N \sigma_{\ln}) \tag{19}$$

$$\Delta t_{fm} = \exp(\mu'_{\ln} + Z_N \sigma'_{\ln}) + \frac{at_0}{R_{\text{diff}} erfc^{-1}(U_{01})} \tag{20}$$

where U_{01} is a random number drawn from a uniform distribution between 0 and 1; R_{diff} is a retardation factor that expresses the delay stemming from matrix diffusion; Z_N is a random number drawn from a normal deviate; $\mu_{\ln}$ and $\sigma_{\ln}$ are the mean and deviation of particle travel time without matrix diffusion, respectively; $\mu'_{\ln}$ and $\sigma'_{\ln}$ are the mean and deviation of particle travel time with matrix diffusion, respectively. The details of computing, Δt_f, Δt_{fm} and other parameters can be found in Delay and Bodin (2001) and Bodin et al. (2003, 2007).

Based on the "SOLFRAC" program (Bodin et al., 2007) and UDEC code, the CAS team developed a FISH code "TDRW_PACKAGE" integrating with UDEC. After the stress-flow calculation, the distribution of fluid flow rates in DFN was extracted into output files. Meanwhile, the connected segments among fractures can be obtained with the inner model data of DFN in UDEC. At last, the TDRW_PACKAGE was used to do the simulation of solute transport.

4. Comparison of transport results

We compare the model characterization and simulation results, by focusing on the breakthrough curves and other transport measurement parameters for macroscopically horizontal flow. The results for macroscopically vertical flow, which are consistent with the results for macroscopically horizontal flow, are not shown here to save space.

4.1. Model characterization by teams

Based on the modeling approaches described in Section 3 and Table 2, we can conclude that a wide range of modeling approaches have been applied, including various types of discontinuum and continuum approaches for modeling of fractured rocks, various methods to consider the effect of stress on permeability, as well as both particle tracking and solute transport modeling. The various teams used the same basic input geometry and properties as defined in the BMT description summarized in Section 2. During the course of this exercise, some simplifications of the fracture network were attempted by several teams. For example, some teams tried to use simplified fracture networks by neglecting short fractures. However, in this problem the short fractures are plentiful and well connected, and are therefore an important contributor to the total flow and transport through the model. Moreover, they might be significant for the mechanical deformation behavior and for potential rock mass failure. Even so, some simplification still could be done,

such as in the case of the KTH and CAS teams. In the end for the final modeling presented in this paper, the IC model and TUL model used the original fracture system without any simplifications. The KTH and CAS teams respectively simplified the model by including 5968 and 6691 fractures so as to guarantee that areas of the blocks were large enough to avoid over-penetration errors in UDEC (Fig. 1b). The LBNL team used the original fracture network for calculation of equivalent, dual-continuum properties.

The mechanical and hydraulic boundary conditions were equivalently applied by all teams as defined in the task definition. For the transport calculation, the IC and the teams (KTH and CAS) injected respectively 1000 and 10,000 particles at the upstream boundary. The TUL and LBNL, using solute transport approach (not particle tracking) equivalently represented the initial and boundary conditions as: (1) zero initial concentration in the whole model; (2) short interval of constant concentration at the inlet boundary, which was consistent with the number of particles proportional to the flow rate; and (3) zero concentration inflow in the later time, in whole boundaries, including the lateral sides parallel to the macroscopic flow direction.

All the teams adopted an aperture change with normal and shear stresses across fractures according to, or closely following, the hyperbolic relation in Eq. (2) with the shear dilation correction according to Eq. (3). However, three of the five teams used simplified stress projection from applied boundary stresses to calculate the normal and shear stresses across each fracture plane to consider stress effects on aperture and permeability. The KTH and CAS teams used UDEC models that performed a complete geomechanical analysis to consider complex interaction between fractures. In particular, the shearing of individual fractures (if significant in this particular problem) would likely be much better captured in UDEC analysis. This is because shearing of an individual fracture is affected by the stiffness of the surrounding fractured medium, but shearing could also become localized in a shear failure propagating along several fractures in the network. The simplified stress projection approach adopted by IC, TUL and LBNL is likely only to be adequate for relatively small shear displacement values that are limited to individual fractures without shear failure propagation in the rock mass.

4.2. Advection comparison for three outlet boundaries

The initial comparison regarding the advection was done with outflow allowed at three outlet boundaries. The simulation results for the case of horizontal flow along a relatively high horizontal gradient are compared in terms of breakthrough curves in Fig. 10, and transport parameters in Table 3. When $K=0$, the breakthrough curves given by each team were quite close, regardless of the flow direction or boundaries. For example, Fig. 9a shows breakthrough curves that plot almost on top of each other for different teams, and Table 3 indicates around 80% particles through the downstream boundary for all teams. This indicates that the transport methods used by different teams could predict similar results for conservative tracers, provided that the configuration of fracture system was the same. In addition, it also validated the simplification of the fracture system adopted by KTH and CAS, as well as the dual-continuum approach adopted by LBNL.

When considering the stress effects, IC, KTH, LBNL and CAS predicted a general trend of a shift of breakthrough curves in the longer time direction with increasing stress ratios. TUL_1 showed a significant backward shift of breakthrough curves, when $K=5$ (see Fig. 10d). TUL_1 predicted the average residence time decreased when $K=5$ for horizontal flow, but other three teams predicted the increasing average residence time with increasing stress ratios (Table 3).

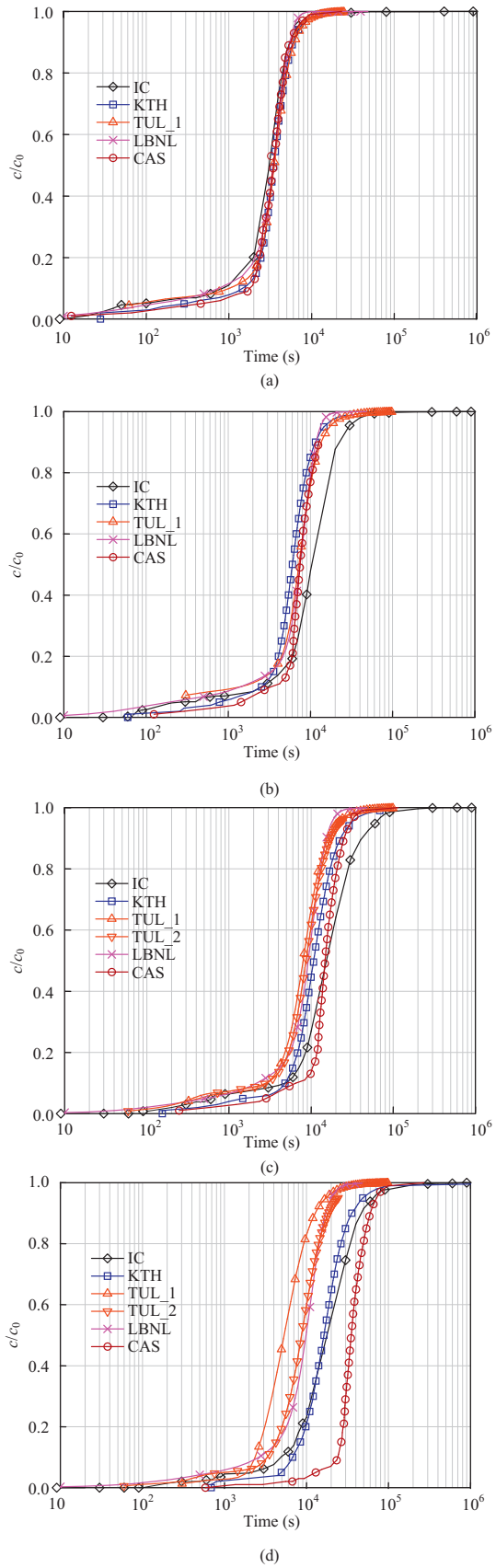

Fig. 10. Comparison of breakthrough curves for conservative tracers exiting from all the three outlet boundaries with increasing stress ratio, under horizontal hydraulic gradient of 10^4 Pa/m (1 m/m). (a) $K=0$. (b) $K=1$. (c) $K=3$. (d) $K=5$.

Table 3
Comparison of results of noninteracting tracers for model with three outlet boundaries under horizontal hydraulic pressure gradient of 10^4 Pa/m (1 m/m) with increasing stress ratio.

Team	Mean water residence time (s)			
	$K=0$	$K=1$	$K=3$	$K=5$
IC	3.73×10^3	1.24×10^4	2.14×10^4	2.59×10^4
KTH	3.81×10^3	7.07×10^3	1.51×10^4	2.53×10^4
TUL_1	4.31×10^3	8.82×10^3	9.34×10^3	6.55×10^3
TUL_2			1.04×10^4	9.90×10^3
LBNL	3.59×10^3	7.55×10^3	9.55×10^3	1.04×10^4
CAS	3.73×10^3	8.50×10^3	1.68×10^4	3.99×10^4
Team	Variance of water residence time (s^2)			
	$K=0$	$K=1$	$K=3$	$K=5$
IC	1.04×10^8	2.13×10^8	5.80×10^8	1.76×10^9
KTH	9.16×10^6	5.08×10^7	6.61×10^9	5.15×10^{10}
TUL_1	4.20×10^6	1.33×10^7	1.82×10^7	1.65×10^7
TUL_2			1.83×10^7	2.21×10^7
LBNL	3.03×10^6	1.45×10^7	2.67×10^7	3.74×10^7
CAS	6.54×10^8	3.82×10^9	1.50×10^{10}	8.42×10^{10}
Team	Percentage of particle from downstream boundary (%)			
	$K=0$	$K=1$	$K=3$	$K=5$
IC	78	76	79	83
KTH	81	80	81	84
TUL_1	79	74	75	83
TUL_2			73	75
LBNL	79	79	79	80
CAS	76	78	78	83

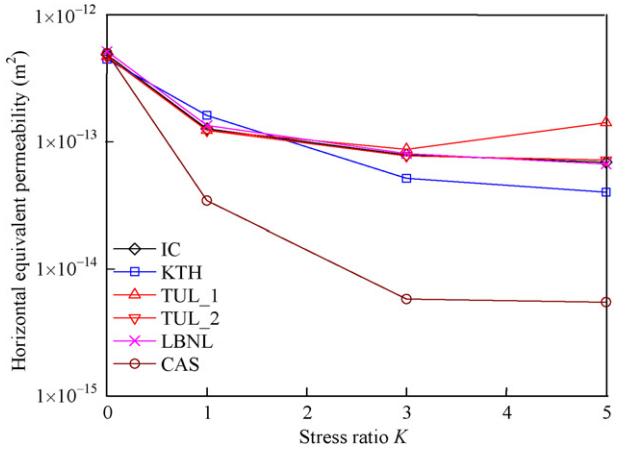

Fig. 11. Comparison of equivalent permeability for horizontal flow at different stress ratios. The results for TUL are that for TUL_1 with a relatively low shear stiffness leading to more substantial shear dilation at a stress ratio of 5.

Together with the divergence of breakthrough curves, it indicates that the mechanical model would have an important influence on flow and transport results. The divergences among four teams could be induced by the different stress–displacement models or parameters of single fracture used by different teams. In fact, the relatively faster breakthrough at $K=5$ for the TUL team can be directly related to the total flow rate or equivalent permeability of the fractured media. For example, Fig. 11 shows that the equivalent permeability calculated from the steady-state flow rate at $K=5$ was much higher than that for TUL_1, because of more significant shear dilation in their model simulation. Other teams did obtain a very small shear dilation effect on permeability and therefore ended up with lower flow rate.

Because a few small fractures located in the boundary area were removed in the KTH and CAS models, the number of possible paths of particle exiting along the lateral boundaries was decreased. Therefore, the beginning parts of breakthrough curves obtained by KTH and CAS were slightly lower than those of breakthrough curves obtained by IC, TUL and LBNL (Fig. 10). The percentages of particle exiting from downstream boundary obtained by KTH were larger than those predicted by other teams too (Table 3), due to the same reason.

4.3. Matrix diffusion comparison

The results for cases including matrix diffusion under a high hydraulic gradient of 10^4 Pa/m were demonstrated to be very similar to that for the conservative tracers, because matrix diffusion only has very minor influence on the transport process. Here, we pay more attention to the cases under lower hydraulic pressure gradient of 10 Pa/m (Fig. 12). IC, KTH, LBNL and CAS completed the simulations of matrix diffusion, whereas in the TUL approaches it is not available to include matrix diffusion at present. The breakthrough curves obtained by CAS did not have longer tails, but the other three teams obtained similar breakthrough curves especially for cases without stress applied. The minor divergences for cases with stress applied could result from the different mechanical models to a large extent. However, the general trends of the breakthrough curves shifting with increasing stress ratios were the same as advection in Section 4.2. The much longer tails for breakthrough curves considering matrix diffusion indicate that a portion of particles might stay in the matrix micropores for a long time to diffuse back to the fractures.

4.4. One outlet boundary case

The models with impermeable lateral boundaries are also of interests, which can be found mostly in the literature and experiments. The basic influence of stress on the transport results is similar to the model with three outlet boundaries, and some of the important issues are summarized below.

The initial step increase in concentration on the breakthrough curves in the case of three outlet boundaries was not observed in the case of one outlet boundary (Fig. 13). In the case of three outlet boundaries, the initial concentration increase is caused by breakthrough at top and bottom boundaries (in the case of horizontal flow) and this could not occur in the case of one outlet boundary.

For conservative tracers, all four teams predicted satisfactory results for the original model without stress impact. The values of average residence time were also close, but significant divergence existed among the Péclet numbers from different teams (Table 4).

The Péclet number determined by Levenspiel (1972) was

$$Pe = \frac{2\bar{t}_w^2}{\sigma_t^2} \tag{21}$$

where $\bar{t}_w$ is the average water residence time, and σ_t is the standard deviation of the water residence time. Moreover, the Péclet numbers for each team varied differently for different stress ratios. There is a general trend of decreasing Péclet numbers at high stress ratios, which indicates that macro-dispersion became more important due to stress-induced channeling. The Péclet numbers estimated by IC, KTH and CAS were much smaller compared with those predicated by TUL and LBNL. The high Péclet number in the LBNL simulation results can be explained by the fact that the macro-dispersion as a result of discrete fracture flow paths is smoothed out in the equivalent continuum approach. This can also explain why the breakthrough curves for the LBNL teams were often sharper

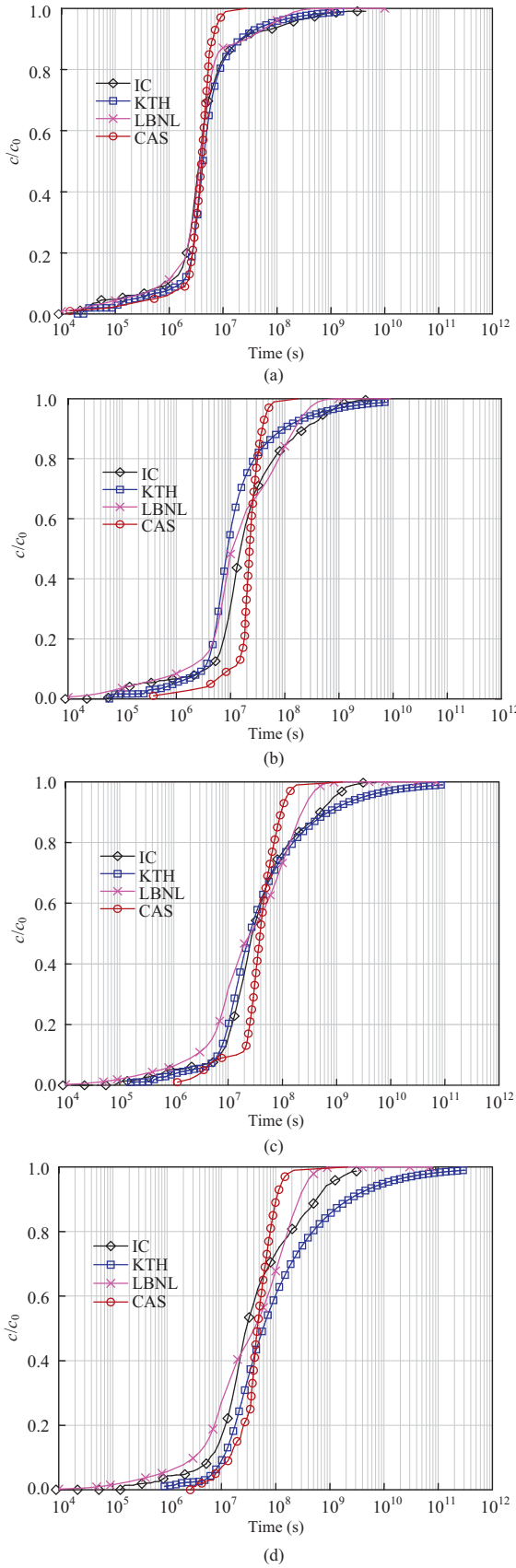

Fig. 12. Comparison of breakthrough curves for interacting tracers exiting from all the three outlet boundaries with increasing stress ratio, under horizontal hydraulic gradient of 10 Pa/m (0.001 m/m). (a) $K = 0$. (b) $K = 1$. (c) $K = 3$. (d) $K = 5$.

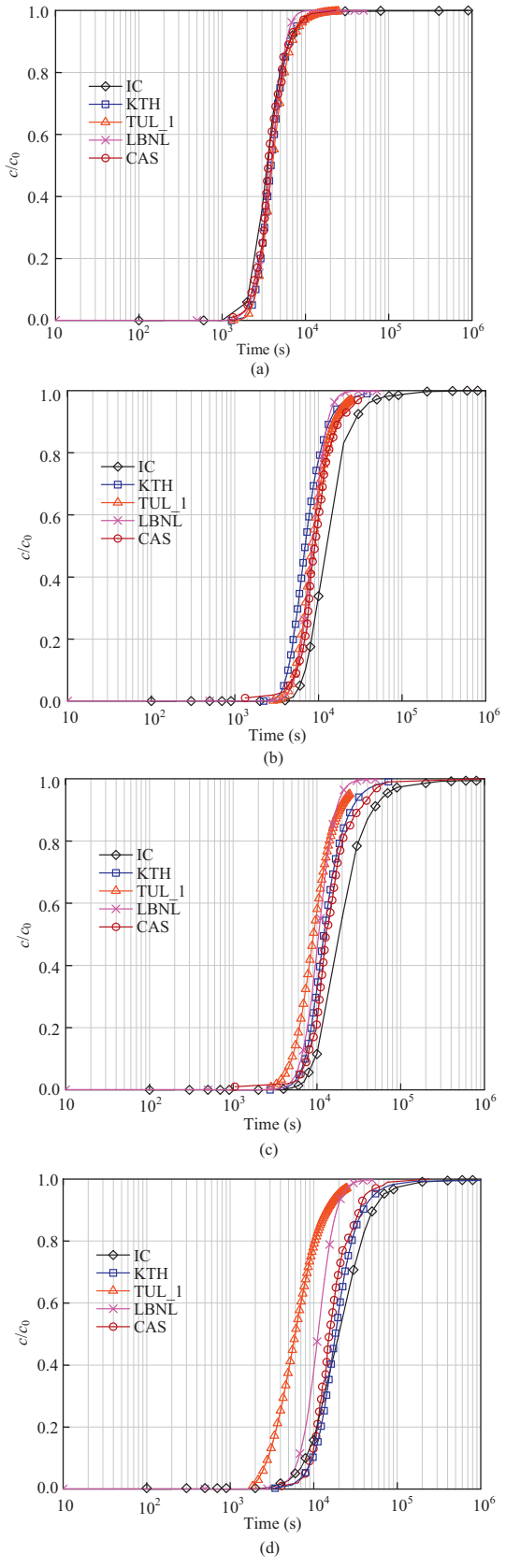

Fig. 13. Comparison of breakthrough curves for conservative tracers exiting from one outlet boundary with increasing stress ratio, under horizontal hydraulic gradient of 10^4 Pa/m (1 m/m). (a) $K = 0$. (b) $K = 1$. (c) $K = 3$. (d) $K = 5$.

Table 4
Comparison of results of non-interacting tracers for model with one outlet boundary under horizontal hydraulic pressure gradient of 10^4 Pa/m (1 m/m) with increasing stress ratio.

Team	Mean water residence time (s)			
	$K=0$	$K=1$	$K=3$	$K=5$
IC	4.62×10^3	9.01×10^3	3.06×10^4	3.98×10^4
KTH	4.40×10^3	7.07×10^3	1.73×10^4	3.08×10^4
TUL_1	4.53×10^3	9.24×10^3	9.81×10^3	7.05×10^3
LBNL	4.29×10^3	9.17×10^3	1.15×10^4	1.25×10^4
CAS	4.28×10^3	1.14×10^4	2.59×10^4	2.14×10^4
Team	Variance of water residence time (s^2)			
	$K=0$	$K=1$	$K=3$	$K=5$
IC	2.44×10^8	5.48×10^8	9.32×10^9	2.82×10^{10}
KTH	9.61×10^6	2.92×10^8	2.19×10^{10}	1.04×10^{11}
TUL_1	4.84×10^6	1.51×10^7	2.01×10^7	1.87×10^7
LBNL	1.95×10^6	1.01×10^7	2.34×10^7	3.62×10^7
CAS	6.86×10^6	7.92×10^7	8.58×10^9	6.43×10^8
Team	Péclet number			
	$K=0$	$K=1$	$K=3$	$K=5$
IC	0.18	0.30	0.20	0.11
KTH	4.04	0.34	0.03	0.02
TUL_1	8.45	11.32	9.59	5.30
LBNL	18.88	16.6	11.37	8.66
CAS	5.34	3.28	0.16	1.42

than those for the other teams that used explicit representation of fractures in their models.

5. Discussions and concluding remarks

IC, KTH, TUL, LBNL and CAS established their own mathematical foundation and numerical models for simulating coupled stress-flow-transport processes in fracture systems, respectively. The comparisons among the results for the same BMT problem obtained from various teams demonstrated that stresses play an important role in solute transport in fractured rocks, which should be carefully reviewed for performance and safety assessments of underground radioactive waste repositories as a potentially important issue. Although minor discrepancies of varying significance still exist among the results from the different teams, this study provided the basic understanding and established the data basis for simulating coupled stress-flow-transport processes in fractured rocks.

For the current fracture network geometry without stress impact, similar results were predicated by all teams for pure advection and matrix diffusion. This demonstrates that both discontinuum and continuum models can generate reasonable results for solute transport. However, for the cases with applied stress, the discrepancies appeared in the results obtained by various teams. Regarding cases with stress applied, the most significant difference occurred at the high stress ratio of 5, when in particular the TUL team achieved a much faster breakthrough. This was identified as being caused by a more significant shear dilation, which can be directly related to a relatively softer equivalent shear stiffness applied in their analysis. However, interestingly, the analyses by KTH and CAS using UDEC, as well as IC and LBNL, indicated very little effect of shear dilation. This shows that closure of fractures under increasing normal stress was the most important mechanisms for stress-induced changes in permeability in this case. Shear had very small impact, despite that the stress ratio was increased to an extreme value of 5. IC, KTH and CAS used DFN models, but the differences among their results with stress existed. Fig. 14 shows an example of the stress concentrations in a small area of the KTH

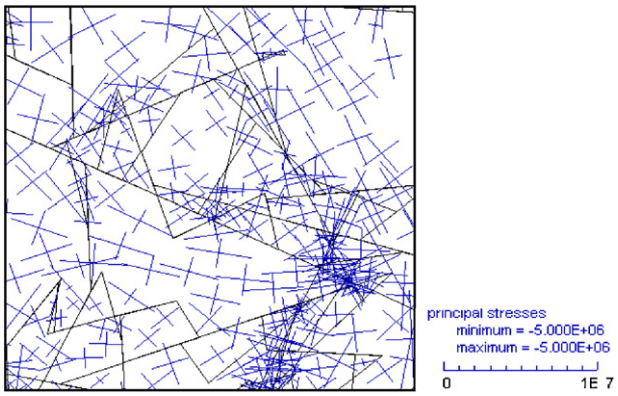

Fig. 14. Stress field of a small zone in Task C model obtained by UDEC under $K=1$.

model when $K=1$. This could be one of the reasons of the discrepancies among the results considering stress effects from different teams, because the highly heterogeneous stress field cannot be considered by the stress projection method. However, to what extent of its influence should be further evaluated in the future study.

One general outstanding issue for DFN models should be mentioned firstly is that the isolated fractures and fracture dead-ends were not considered in the present transport simulation. If only fluid flow is considered, their effects could be negligible. However, their influences on solute transport remain to be further investigated, because in reality the solutes may enter into the stagnant water filled in isolated fracture or dead-ends by molecular diffusion.

Average residence time is not necessarily an accurate measurement of the transport results, because it is easily influenced by a few particles with extremely large residence time. Consequently, the time when 50% particles passed the outlet boundaries may be a more proper evaluation parameter. The value of the Péclet number in reality is often found to vary between 1 and 100 in fractured rocks (Gelhar, 1993), and the Péclet numbers from TUL, LBNL and CAS are within this range. The possible reason for the small Péclet number is that the variance of water residence time could be strongly influenced by the tails of the breakthrough curves. To avoid the Péclet number dominated by the breakthrough tails, an alternative method proposed by Kobayashi et al. (2001) is employed to estimate the Péclet number based on the arrival time for $c/c_0=0.1$, 0.5 and 0.9.

The results show a need for research on effect of hydraulic boundary condition on advection, and more importantly on matrix diffusion under relatively low hydraulic pressure gradient. If the pressure gradient is about 10^4 Pa/m, then there is no need to account for RMD for the current fracture system because of its minimal effect. The importance of matrix diffusion largely depends on the flow wetted surface and flow rate, and different hydraulic boundary conditions can induce different flow rates and paths. Even though matrix diffusion dominates the solute residence time for low hydraulic gradient, the particle tracking procedures are still required to account for the differences in residence times between the different paths. The IC team found that the diffusion distance in the RMD model became a key parameter when the pressure gradient is reduced to a relatively small level, say 10^{-2} Pa/m in this study (Fig. 15), and the breakthrough curve for a diffusion distance of 0.1 m was significantly different from that for a diffusion distance of 10 m. However, the latter one is similar to the results obtained using KTH (project specified) method, presumably because of 10 m to all intents and purposes corresponding to an infinite diffusion distance.

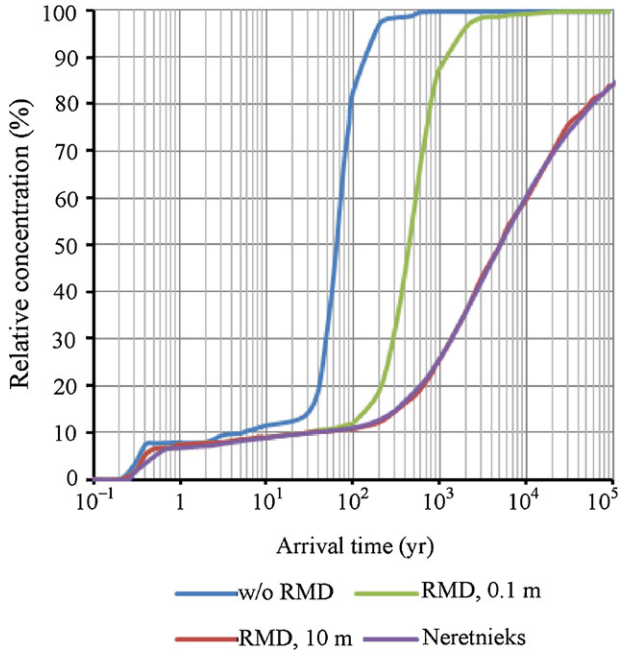

Fig. 15. The effect of diffusion distance under vertical pressure gradient of 10^{-2} Pa/m.

The above outstanding issues are not unique to the problems studied in this project, but are valid as general outstanding issues in coupled HMC problems in fractured rocks in general, and fractured crystalline rocks in particular. They can serve as starting points for future research during and beyond the current stage of DECOVALEX-2011.

Acknowledgements

The work described in this paper was conducted within the context of the international DECOVALEX-2011 Project. The authors are grateful to the Funding Organizations who supported the work: Royal Institute of Technology (KTH), was supported by Swedish Nuclear Fuel and Waste Co. (SKB), Sweden; Technical University of Liberec (TUL), was supported by Radioactive Waste Repository Authority (RAWRA), Czech Republic; Imperial College London (IC) and Lawrence Berkeley National Laboratory (LBNL), in collaboration with Serco TAS were supported by Nuclear Decommissioning Authority (NDA), UK. The support to LBNL from NDA via SERCO TAS was provided through the U.S. Department of Energy Contract No. DE-AC02-05CH11231. The TUL team was further supported by the Ministry of Education of the Czech Republic within the SGS project No. 7822/115 on the TUL. The views expressed in the paper are however, those of the authors and are not necessarily those of the Funding Organizations.

References

Baghbanan A, Jing L. Hydraulic properties of fractured rock masses with correlated fracture length and aperture. International Journal of Rock Mechanics and Mining Sciences 2007;44(5):704–19.

Baghbanan A, Jing L. Stress effects on permeability in fractured rock masses with correlated fracture length and aperture. International Journal of Rock Mechanics and Mining Sciences 2008;45(8):1320–34.

Bai M, Elsworth D. Modeling of subsidence and stress-dependent hydraulic conductivity for intact and fractured porous media. Rock Mechanics and Rock Engineering 1994;27(4):209–34.

Bai M, Meng F, Elsworth D, Roegiers JC. Analysis of stress-dependent permeability in nonorthogonal flow and deformation fields. Rock Mechanics and Rock Engineering 1999;32(3):195–219.

Bodin J, Porel G, Delay F. Simulation of solute transport in discrete fracture networks using the time domain random walk method. Earth and Planetary Science Letters 2003;208(3/4):297–304.

Bodin J, Porel G, Delay F, Ubertosi F, Bernard S, de Dreuzy JR. Simulation and analysis of solute transport in 2D fracture/pipe networks: the SOLFRAC program. Journal of Contaminant Hydrology 2007;89(1/2):1–28.

Chen M, Bai M. Modeling stress-dependent permeability for anisotropic fractured porous rocks. International Journal of Rock Mechanics and Mining Sciences 1998;35(8):1113–9.

Cordes C, Kinzelbach W. Continuous groundwater velocity fields and path lines in linear, bilinear, and trilinear finite elements. Water Resources Research 1992;28(11):2903–11.

Delay F, Bodin J. Time domain random walk method to simulate transport by advection–dispersion and matrix diffusion in fracture networks. Geophysical Research Letters 2001;28(21):4051–4.

Dieterich JH, Linker MF. Fault stability under conditions of variable normal stress. Geophysical Research Letters 1992;19(16):1691–4.

Gelhar LW. Stochastic subsurface hydrology. New York: Prentice Hall; 1993.

Genty A, Potier CL, Gounand S. Analysis of the excavation deviations impact on geological radioactive waste repository performance. Geotechnical and Geological Engineering 2011;29(4):537–54.

Gylling B, Moreno L, Neretnieks I. The channel network model – a tool for transport simulations in fractured media. Ground Water 1999;37(3):367–75.

Hoch AR. Implementation of a rock-matrix diffusion model in the discrete fracture network code NAPSAC. Nirex: Nirex Science Report S/98/005; 1998.

Hudson JA, Tsang CF, Jing L, Andersson JC. The DECOVALEX coupled modeling project—past, present and future. In: Proceedings of the ISRM-sponsored International Symposium on Rock Mechanics—Rock Characterisation, Modeling and Engineering Design Methods. Hong Kong: International Society for Rock Mechanics; 2009. p. 933–7.

Itasca Consulting Group, Inc. UDEC 4.0 user's guide. Minneapolis, Minnesota: Itasca Consulting Group, Inc; 2004.

Itasca Consulting Group, Inc. FLAC3D, fast Lagrangian analysis of continua in 3 dimensions (version 4.0). Minneapolis, Minnesota: Itasca Consulting Group, Inc; 2009.

Jackson CP, Hoch AR, Todman S. Self-consistency of a heterogeneous continuum porous medium representation of a fractured medium. Water Resources Research 2000;36(1):189–202.

Jeong W, Song J. Numerical investigation for flow and transport in a rough fracture with hydromechanical effect. Energy Sources 2005;27(11):997–1011.

Kim J, Sonnenthal E, Rutqvist J. Formulation and sequential numerical algorithms of coupled fluid/heat flow and geomechanics for multiple porosity materials. International Journal for Numerical Methods in Engineering 2012;92(5):425–56.

Kobayashi A, Fujita T, Chijimatsu M. Continuous approach for coupled mechanical and hydraulic behavior of a fractured rock mass during hypothetical shaft sinking at Sellafield, UK. International Journal of Rock Mechanics and Mining Sciences 2001;38(1):45–57.

Koyama T, Fardin N, Jing L, Stephansson O. Numerical simulation of shear induced flow anisotropy and scale dependent aperture and transmissivity evolutions of fracture replicas. International Journal of Rock Mechanics and Mining Sciences 2006;43(1):89–106.

Koyama T, Li B, Jiang Y, Jing L. Numerical simulations for the effects of normal loading on particle transport in rock fractures during shear. International Journal of Rock Mechanics and Mining Sciences 2008;45(8):1403–19.

Levenspiel O. Chemical reaction engineering. 2nd ed. New York: Wiley; 1972. p. 566.

Maryška J, Severýn O, Tauchman M, Tondr D. Modelling of processes in fractured rock using FEM/FVM on multidimensional domains. Journal of Computational and Applied Mathematics 2008;215(2):495–502.

Min KB, Jing L, Stephansson O. Fracture system characterization and evaluation of the equivalent permeability tensor of fractured rock masses using a stochastic REV approach. Hydrogeology Journal 2004a;12(5):497–510.

Min KB, Rutqvist J, Tsang CF, Jing L. Stress-dependent permeability of fractured rock masses: a numerical study. International Journal of Rock Mechanics and Mining Sciences 2004b;41(7):1191–210.

Moreno L, Tsang YW, Tsang CF, Hale FV, Neretnieks I. Flow and tracer transport in a single fracture: a stochastic model and its relation to some field observation. Water Resources Research 1988;24(12):2033–48.

Moreno L, Crawford J, Neretnieks I. Modeling radionuclide transport for time varying flow in a channel network. Journal of Contaminant Hydrology 2006;86(3/4):215–38.

Neretnieks I, Tsang CF, Moreno L. Particle transport simulation scheme for non-interacting and interacting tracers. Royal Institute of Technology, Sweden: DECOVALEX-2011 Project Secretariat, Internal Project Document, 2009.

Oda M. An equivalent continuum model for coupled stress and fluid flow analysis in jointed rock masses. Water Resources Research 1986;23(13):1845–56.

Pruess K, Narasimhan TN. A practical method for modeling fluid and heat flow in fractured porous media. Society of Petroleum Engineers (SPE) Journal 1985;25(1):14–26.

Pruess K, Oldenburg C, Moridis G. TOUGH2 user's guide, report LBNL-43134. Version 2.0. Berkeley, California Lawrence Berkeley National Laboratory; 1999, p. 198.

Rahman MK, Hossain MM, Rahman SS. A shear-dilation-based model for evaluation of hydraulically stimulated naturally fractured reservoirs. International Journal for Numerical and Analytical Methods in Geomechanics 2002;26(5):469–97.

Rutqvist J, Wu YS, Tsang CF, Bodvarsson G. A modeling approach for analysis of coupled multiphase fluid flow, heat transfer, and deformation in fractured

porous rock. International Journal of Rock Mechanics and Mining Sciences 2002;39(4):429–42.
Rutqvist J, Bäckström A, Chijimatsu M, Feng XT, Pan PZ, Hudson J, et al. A multiple-code simulation study of the long-term EDZ evolution of geological nuclear waste repositories. Environmental Geology 2009;57(6):1313–24.
Rutqvist J. Status of the TOUGH-FLAC simulator and recent applications related to coupled fluid flow and crustal deformations. Computers and Geosciences 2011;37(6):739–50.
Serco TAS. NAPSAC technical summary: release 9.6. Serco TAS: Serco Report SA/ENV/CONNECTFLOW/12; 2008.
Technical University of Liberec (TUL). FLOW123D v1.6.5, Documentation of file formats and brief user manual, Liberec, Czech Rep, NTI TUL; 2011. http://dev.nti.tul.cz/~brezina/flow_doc/flow123d_manual.pdf
Waber HN, Gimmi T, Smellie JAT. Effects of drilling and stress release on transport properties and porewater chemistry of crystalline rocks. Journal of Hydrology 2011;405(3/4):316–32.
Yamashita R, Kimura H. Particle-tracking technique for nuclide decay chain transport in fractured porous media. Journal of Nuclear Science and Technology 1990;27(11):1041–9.
Zhang X, Sanderson DJ. Effects of stress on the 2-D permeability tensor of natural fracture networks. Geophysics Journal International 1996;125(3):912–24.
Zhao Z, Jing L, Neretnieks I, Moreno L. Numerical modeling of stress effects on solute transport in fractured rocks. Computers and Geotechnics 2011;38(2):113–26.
Zimmerman RW, Bodvarsson GS. Hydraulic conductivity of rock fractures. Transport in Porous Media 1996;23(1):1–30.